224771: kyanite-bearing garnet semipelitic schist, Kingsley prospect

(South West Terrane, Yilgarn Craton)

Kelsey, DE, Korhonen, FJ, Blereau, ER, Romano, SS, Fielding, IOH and De Paoli, M

Location and sampling

Pemberton (SI 50-10), Donnelly (2029)

MGA Zone 50, 407640E 6219876N

Warox Site MDPPEM000003

Sampled on 13 April 2017 (date entered)

This sample was collected from the 205.83 – 205.96 m depth interval of diamond drillcore WPD02, drilled in 2003 by Teck Caminco Australia Pty Ltd at the Kingsley prospect of their Wheatley project (Johnston, 2003). The drillhole is located about 25 km south-southwest of Bridgetown, 16.6 km west-northwest of Manjimup and 8.1 km east-southeast of Mount Mack.

Geological context

The unit sampled is a semipelitic schist (Fig. 1) from the southwestern corner of the South West Terrane of the Yilgarn Craton (Quentin de Gromard et al., 2021), within a belt of Archean metasedimentary and gneissic rocks informally referred to by Wilde et al. (2001) as the Balingup metamorphic belt. Granitic and gneissic rocks along the western margin of the Yilgarn Craton have yielded U–Pb zircon dates of 2.68 – 2.61 Ga (e.g. Nelson, 2004; Nemchin and Pidgeon, 1997; Lu et al., 2015). The sample locality is about 23 km east of the Darling Fault, a >1000 km long structure that forms the boundary between Precambrian rocks of the Yilgarn Craton and Paleozoic and younger rocks of the Perth Basin. The Darling Fault may have been initiated during the Archean (Blight et al., 1981), and was active during the Proterozoic and Phanerozoic, and possibly into the Neogene (Thomas, 2014). Monazite from the sample reported here yielded dates of 1148 ± 5 Ma and 1037 ± 9 Ma, with both groups interpreted as metamorphic ages (GSWA 224771, Fielding et al., 2022). Monazite from drillcores 1.2 and 1.5 km to the west-southwest indicate discrete episodes of metamorphism or hydrothermal fluid flow at c. 1840, 1190, 1145 and 1040 Ma (GSWA 224767, 224777, 224779, preliminary data). Zircon in amphibolite from the same drillcore as GSWA 224767, located 1.5 km to the southwest, yields a date of 1179 ± 6 Ma (GSWA 229286, Wingate et al., 2021) and is likely a metamorphic age. Geoscience Australia sample 2004968001A, composed dominantly of recrystallized quartz, microcline, plagioclase and micas taken from the depth interval 235.22 – 237.05 m in the current diamond drillhole, yielded U–Pb SHRIMP zircon dates between c. 2700 to 2600 Ma with a prominent age component at c. 2646 Ma interpreted as the maximum age of deposition (Sircombe et al., 2007; Hassan 2017).

Petrographic description

The sample is a semipelitic schist (Fig. 1) containing about 33% plagioclase, 31% quartz, 26% biotite, 8% garnet, 2% kyanite, 1% muscovite and trace amounts of apatite, staurolite, chlorite, monazite, zircon, ilmenite, rutile, tourmaline, arsenopyrite, pyrrhotite, and Ni–Co–Fe–As-sulfide (Fig. 2; Table 1). Plagioclase is up to 2.5 mm in diameter and occurs within the matrix predominantly with biotite but also with quartz and kyanite (Figs 2, 3). Anhedral quartz, up to 3 mm in diameter, occurs dispersed throughout the biotite–plagioclase matrix and also occurs as discontinuous, undulating layers (Fig. 2) intergrown with plagioclase, kyanite and biotite and as inclusions within garnet porphyroblasts. Biotite laths, up to 1.5 mm in length, define the foliation and layering with plagioclase. The biotite–plagioclase±quartz-rich aggregate layers wrap around garnet, and uncommonly biotite is concentrated in the strain shadows of garnet. Rarer grains of biotite are highly discordant to the main fabric and may be post-peak. Garnet porphyroblasts

are equant (up to 3 mm in diameter) to oblong (up to 7 mm in diameter) with anhedral grain boundaries (Figs 1–3). Some garnet rims have higher concentration of small inclusions of quartz, making those rims texturally distinct from the cores. Garnet cores contain inclusions of quartz and rare inclusions of biotite, apatite, staurolite, ilmenite and plagioclase (Fig. 2). Garnet rims are in some cases more inclusion-rich than cores and contain fine-grained inclusions of kyanite, staurolite, quartz, biotite, plagioclase and apatite. Kyanite occurs as trails of small anhedral to prismatic–subhedral grains (up to 2 mm in length) within the biotite–plagioclase–quartz-bearing matrix (Figs 2, 3) as well as typically finer grained inclusions in the rims of garnet. Rare, tiny (up to ~130 µm, typically ≤50 µm long) grains of staurolite occur throughout the matrix. Muscovite occurs as acicular to prismatic grains amongst the biotite-rich matrix and ranges from concordant to highly discordant to the biotite-rich foliation. The highly discordant muscovite may be post-peak. Ilmenite occurs as rare, tiny grains most commonly as inclusions in garnet, but also in the matrix. Rutile occurs as very rare, tiny grains in the matrix. Sulfides mainly occur as isolated, disseminated grains within a particular ~2.5 mm wide horizon of matrix in the sample.

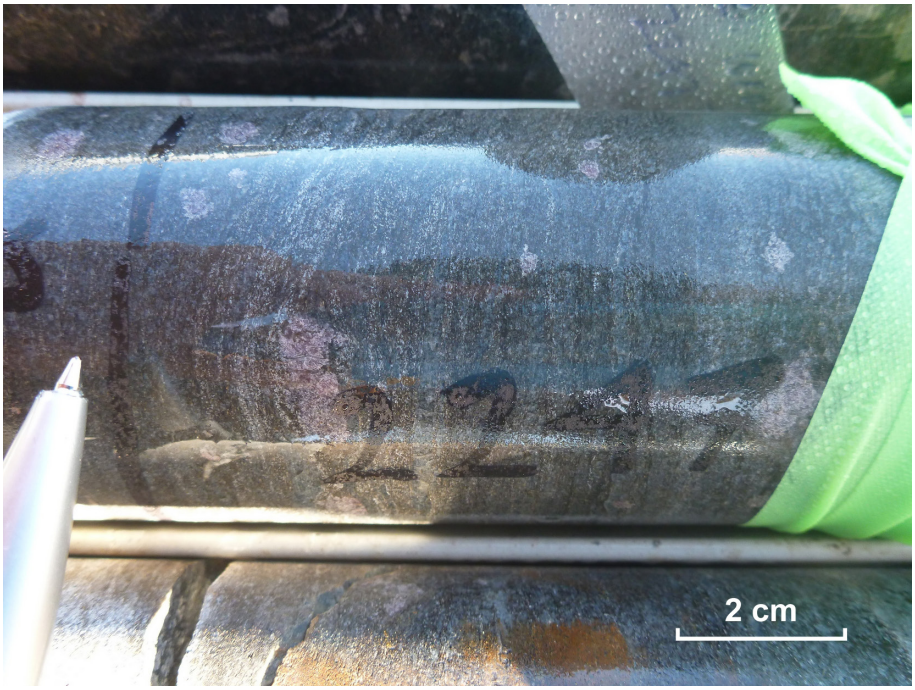

Figure 1. **Drillcore image of sample 224771: kyanite-bearing garnet semipelitic schist, Kingsley prospect**

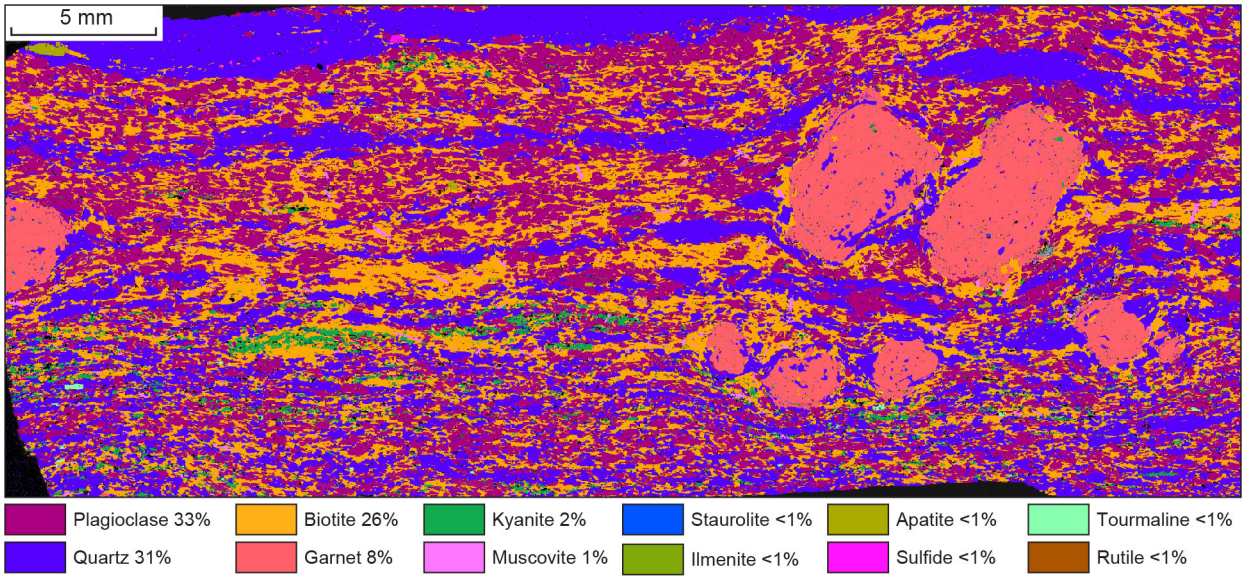

Figure 2. **TESCAN Integrated Mineral Analyser (TIMA) image of an entire thin section from sample 224771: kyanite-bearing garnet semipelitic schist, Kingsley prospect. Volume percent proportion of major rock-forming minerals are calculated by the TIMA software**

Table 1. Mineral modes for sample 224771: kyanite-bearing garnet semipelitic schist, Kingsley prospect

Mineral modes	*Qz*	*Bt*	*Pl*	*Grt*	*Ky*	*Ms*	*Ap*	*Chl*	*St*	*Ilm*	*Rt*	*Sulfide*[(b)]
Observed (vol%)[(a)]	31	26	33	8	2	1	0.20	0.08	0.05	0.01	0.01	0.1
Predicted (mol%)												
@ 690 °C, 7.7 kbar	32	28	28	7	6	–	–	–	–	<1	–	–
@ 680 °C, 8.7 kbar	31	26	27	8	6	2	–	–	–	<1	–	–
@ 675 °C, 10.2 kbar	30	16	21	16	<1	15	–	–	–	<1	<1	–

NOTES: (a) trace monazite and zircon also present in thin section
(b) sulfides include pyrrhotite, aresnopyrite, Ni-bearing arsenopyrite
– not present

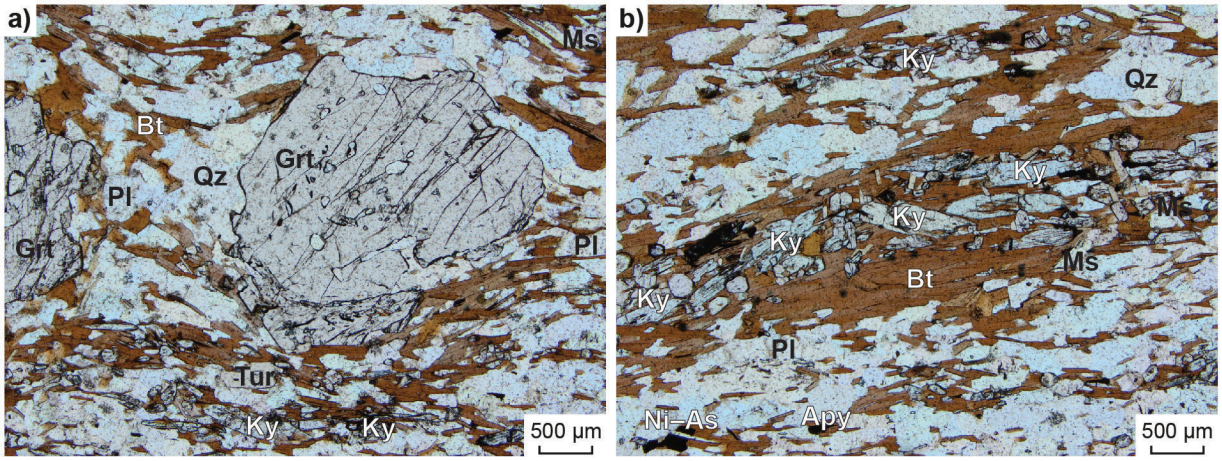

Figure 3. **Photomicrographs, in plane-polarized light, of sample 224771: kyanite-bearing garnet semipelitic schist, Kingsley prospect. Abbreviations: Apy, arsenopyrite; Ni–As, Ni–Co–Fe–As sulphide; Tur, tourmaline. Other mineral abbreviations are explained in the caption to Figure 4**

Analytical details

The metamorphic evolution of this sample was investigated using phase equilibria modelling, based on the bulk-rock composition (Table 2). The bulk-rock composition was determined by X-ray fluorescence spectroscopy, together with loss on ignition (LOI). The modelled O content (for Fe^{3+}) was constrained to be equal to 11% of FeO via exploration of calculated phase equilibria at different oxidation states prior to calculation of the *P–T* pseudosection. The sample is interpreted to be subsolidus and was modelled with H_2O in excess to create hydrated assemblages. As the sample was modelled with H_2O in excess no fields above the solidus were modelled. The bulk composition was corrected for the presence of apatite by applying a correction to CaO (Table 1). Thermodynamic calculations were performed in the MnNCKFMASHTO ($MnO–Na_2O–CaO–K_2O–FeO–MgO–Al_2O_3–SiO_2–H_2O–TiO_2–O$) system using THERMOCALC version tc340 (updated October 2013; Powell and Holland 1988) and the internally consistent thermodynamic dataset of Holland and Powell (2011; dataset tc-ds62, created in February 2012). The activity–composition relations used in the modelling are detailed in White et al. (2014a,b). Raman spectroscopy was conducted to determine which aluminosilicate(s) were present with the sample. Grains selected for Raman analysis covered a range of textural sites, different grain sizes, and the presence of twinning and/or cleavage planes. The analysis identified the aluminosilicate grains as kyanite.

Table 2. Measured whole-rock and modelled compositions for sample 224771: kyanite-bearing garnet semipelitic schist, Kingsley prospect

XRF whole-rock composition (wt%)[a]											
SiO_2	**TiO_2**	**Al_2O_3**	**Fe_2O_3**	**FeO[b]**	**MnO**	**MgO**	**CaO**	**Na_2O**	**K_2O**	**P_2O_5**	**LOI**	**Total**
60.72	0.67	17.07	–	8.20	0.10	3.76	2.11	2.08	2.90	0.09	0.88	98.58
Normalized composition used for phase equilibria modelling (mol%)												
SiO_2	**TiO_2**	**Al_2O_3**	**O[c]**	**FeO^{T}[d]**	**MnO**	**MgO**	**CaO[e]**	**Na_2O**	**K_2O**	**–**	**H_2O[f]**	**Total**
67.32	0.56	11.15	0.42	7.60	0.09	6.22	2.36	2.24	2.05		–	100

NOTES: (a) Data and analytical details are available from the WACHEM database <http://geochem.dmp.wa.gov.au/geochem/>
(b) FeO content is total Fe
(c) O content (for Fe_2O_3) constrained as 11% of total Fe
(d) FeO^T = moles FeO + 2 * moles O
(e) CaO modified to remove apatite: CaO(Mod) = CaO(Total) - (moles CaO(in Ap) = 3.33 * moles P_2O_5)
(f) H_2O content set in modelling as 'in excess', requiring no amount to be explicitly specified in bulk composition

Results

Metamorphic *P–T* estimates have been derived based on detailed examination of one thin section and the bulk-rock composition; care was taken to ensure that the thin section and the sample volume selected for whole-rock geochemistry were similar in terms of featuring the same minerals in approximately the same abundances (Table 1), to minimize any potential compositional differences. The *P–T* pseudosection for sample 224771 was calculated over a temperature range of 600–720 °C and between 5 and 12 kbar (Fig. 4). The solidus is located at 655–703 °C across the range of modelled pressures. Garnet and biotite are stable throughout the *P–T* range. Cordierite is stable below 5.6 kbar, staurolite is stable in a positively sloped region through the central part of the pseudosection, between 5 and 8.8 kbar at 645 °C. Staurolite stability terminates at higher pressures due to the stability of paragonite and at higher temperatures due to the stability of kyanite. Kyanite is stable in a restricted region from 7.4 to 10.4 kbar and from 665 °C to the solidus at 675–690 °C. Magnetite is stable below ~7 kbar; rutile is stable at high pressures and low temperatures, above ~6.9 kbar at 625 °C and above ~8.9 kbar at 680 °C, though at the lowest pressures and temperatures rutile and magnetite coexist. Ilmenite stability terminates above ~9 kbar at 610 °C and above ~11.2 kbar at 660 °C. Epidote and albite are stable at the highest pressures and lowest temperatures in the pseudosection. Sillimanite is stable at the high-temperature–low-pressure corner of the pseudosection, and chlorite is stable at the lowest temperatures modelled.

Interpretation

Based on the coarse grain size and mineral associations that support textural equilibrium, the peak metamorphic assemblage is interpreted to be garnet–kyanite–plagioclase–biotite–ilmenite–quartz–H_2O±muscovite±rutile. Petrographic observations indicate an earlier assemblage that contained staurolite rather than kyanite, whereas muscovite and biotite with an orientation discordant to the main fabric are interpreted as late.

The interpreted peak metamorphic assemblage is stable from 7.5 to 10.4 kbar and 665 °C to the solidus at 675–690 °C (Fig. 4). The peak assemblage is limited by the stability of staurolite to lower temperatures, instability of kyanite at higher pressures, the solidus to higher temperatures and the stability of sillimanite to lower pressure (Fig. 4). The sample was modelled with H_2O in excess as the sample was interpreted to be subsolidus, as opposed to using the measured LOI as the amount of H_2O, which places the solidus at a minimum temperature. Whether muscovite and rutile are interpreted to be part of the peak assemblage affects the *P–T* constraints of the peak assemblage. The small vol% abundance of both muscovite and rutile (Table 1) suggests that maximum, or absolute, pressures were approximately at the rutile-in boundary (Fig. 4).

As staurolite occurs within garnet but is extremely rare in the matrix, it is not interpreted as part of the peak assemblage. However, the transition from a staurolite- to kyanite-bearing assemblage could represent a prograde evolution, though monazite geochronology from this sample defines two distinct age groups, 1148 ± 5 Ma and 1037 ± 9 Ma, both interpreted as metamorphic (GSWA 224771, preliminary data). This could mean that the staurolite-bearing assemblage represents a temporally distinct and older metamorphic

event than the kyanite-bearing assemblage. Monazite of both age groups occurs throughout the matrix and within rims of garnet (garnet is typically monazite-inclusion-poor), and as such there is no microstructural–spatial relationship in the monazite age data to provide a strong link between age and silicate mineral assemblage paragenesis. Therefore, at present it is unclear how to interpret the monazite age data in the context of the *P–T* constraints. There is limited petrological information to constrain any *P–T* path information other than the transition from a staurolite- to kyanite-bearing assemblage.

Peak metamorphic conditions are estimated at 7.5 – 10.4 kbar and 665–690 °C, with an apparent thermal gradient between 65 and 92 °C/kbar. It is unclear whether the earlier staurolite-bearing assemblage represents a temporally distinct and older metamorphic event than the kyanite-bearing assemblage or is part of the prograde evolution.

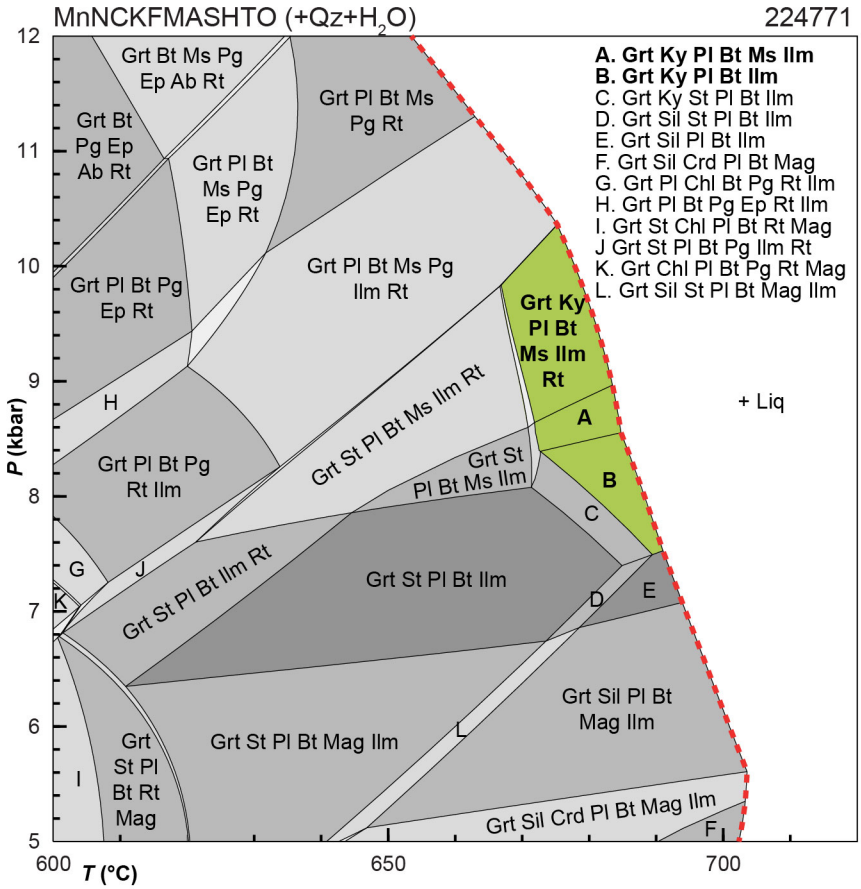

Figure 4. ***P–T*** **pseudosection calculated for sample 224771: kyanite-bearing garnet semipelitic schist, Kingsley prospect. Assemblage fields corresponding to peak metamorphic conditions are shown in bold text and green shading. Red dashed line represents the solidus. Abbreviations: Ab, albite; Bt, biotite; Chl, chlorite; Crd, cordierite; Ep, epidote; Grt, garnet; H_2O, fluid (pure H_2O); Ilm, ilmenite; Ky, kyanite; Liq, silicate melt; Mag, magnetite; Ms, muscovite; Pg, paragonite ; Pl, plagioclase; Qz, quartz; Rt, rutile; Sil, sillimanite; St, staurolite**

References

Blight, DF, Compston, W and Wilde, SA 1981, The Logue Brook Granite, in Annual report for the year 1980: Geological Survey of Western Australia, Perth, Western Australia, p. 72–80.

Cassidy, KF, Champion, DC, Krapež, B, Barley, ME, Brown, SJA, Blewett, RS, Groenewald, PB and Tyler, IM 2006, A revised geological framework for the Yilgarn Craton, Western Australia: Geological Survey of Western Australia, Record 2006/8, 8p.

Fielding, IOH, Wingate, MTD Korhonen, FJ and Rankenburg, K 2022, 224771: kyanite-bearing garnet pelitic schist, Wheatley prospect; Geochronology Record XXXX: Geological Survey of Western Australia, Xp.

Hassan, LY 2017, Metamorphosed VMS mineralization at Wheatley, southwest Western Australia: Geological Survey of Western Australia, Record 2017/9, 39p.

Holland, TJB and Powell, R 2011, An improved and extended internally consistent thermodynamic dataset for phases of petrological interest, involving a new equation of state for solids: Journal of Metamorphic Geology, v. 29, no. 3, p. 333–383.

Johnston, PJ 2003, Annual Report E70/2258, Wheatley Project, 01 June 2002 to 31 May 2003: Mineral Exploration Report A66807 (unpublished), 24p.

Korhonen, FJ, Kelsey, DE, Fielding IOH and Romano, SS 2020, The utility of the metamorphic rock record: constraining the pressure–temperature–time conditions of metamorphism: Geological Survey of Western Australia, Record 2020/14, 24p.

Lu, Y, Wingate, MTD, Bodorkos, S and Wyche, S 2015a, 184115: granite gneiss, Kirup; Geochronology Record 1279: Geological Survey of Western Australia, 4p.

Nemchin, AA and Pidgeon, RT 1997, Evolution of the Darling Range Batholith, Yilgarn Craton, Western Australia: a SHRIMP study: Journal of Petrology, v. 38, p. 625–649.

Powell, R and Holland, TJB 1988, An internally consistent dataset with uncertainties and correlations: 3. Applications to geobarometry, worked examples and a computer program: Journal of Metamorphic Geology, v. 6, no. 2, p. 173–204.

Quentin de Gromard, R, Ivanic, TJ and Zibra, I 2021, Pre-Mesozoic interpreted bedrock geology of the southwest Yilgarn: Geological Survey of Western Australia, digital data layers.

Sircombe, KN, Cassidy, KFC, Champion, DC and Tripp, G 2007, Compilation of SHRIMP U-Pb geochronological data, Yilgarn Craton, Western Australia, 2004-2006: Geoscience Australia, Record 2007/01, 182p.

Thomas, CM 2014, The tectonic framework of the Perth Basin: current understanding: Geological Survey of Western Australia, Record 2014/14, 36p.

White, RW, Powell, R, Holland, TJB, Johnson, TE and Green, ECR 2014a, New mineral activity-composition relations for thermodynamic calculations in metapelitic systems: Journal of Metamorphic Geology, v. 32, no. 3, p. 261–286.

White, RW, Powell, R and Johnson, TE 2014b, The effect of Mn on mineral stability in metapelites revisited: New a–x relations for manganese-bearing minerals: Journal of Metamorphic Geology, v. 32, no. 8, p. 809–828.

Wingate, MTD, Fielding, IOH, Lu, Y, Ivanic, TJ and Quentin de Gromard, R 2021, 229286: amphibolite, Wheatley prospect; Geochronology Record 1793: Geological Survey of Western Australia, 5p.

Wilde, SA 2001, Jimperding and Chittering metamorphic belts, southwestern Yilgarn Craton, Western Australia — a field guide: Geological Survey of Western Australia, Record 2001/12, 24p.

Links

Metamorphic history introduction document: Intro_2020.pdf

Recommended reference for this publication

Kelsey, DE, Korhonen, FJ, Blereau, ER, Romano, SS, Fielding, IOH and De Paoli, M 2022, 224771: kyanite-bearing garnet pelitic schist, Kingsley prospect; Metamorphic History Record 18: Geological Survey of Western Australia, 7p.

Data obtained: 10 March 2020

Date released: 14 April 2022

This Metamorphic History Record was last modified on 29 March 2022.

Grid references in this publication refer to the Geocentric Datum of Australia 1994 (GDA94). All locations are quoted to at least the nearest 100 m.

WAROX is GSWA's field observation and sample database. WAROX site IDs have the format 'ABCXXXnnnnnnSS', where ABC = geologist username, XXX = project or map code, nnnnnn = 6 digit site number, and SS = optional alphabetic suffix (maximum 2 characters).

Isotope and element analyses are routinely conducted using the GeoHistory laser ablation ICP-MS and Sensitive High-Resolution Ion Microprobe (SHRIMP) ion microprobe facilities at the John de Laeter Centre (JdLC), Curtin University, with the financial support of the Australian Research Council and AuScope National Collaborative Research Infrastructure Strategy (NCRIS). The TESCAN Integrated Mineral Analyser (TIMA) instrument was funded by a grant from the Australian Research Council (LE140100150) and is operated by the JdLC with the support of the Geological Survey of Western Australia, The University of Western Australia (UWA) and Murdoch University. Mineral analyses are routinely obtained using the electron probe microanalyser (EPMA) facilities at the Centre for Microscopy, Characterisation and Analysis at UWA, and at Adelaide Microscopy, University of Adelaide.

Digital data related to WA Geology Online, including geochronology and digital geology, are available online at the Department's Data and Software Centre and may be viewed in map context at GeoVIEW.WA.

Disclaimer

This product uses information from various sources. The Department of Mines, Industry Regulation and Safety (DMIRS) and the State cannot guarantee the accuracy, currency or completeness of the information. Neither the department nor the State of Western Australia nor any employee or agent of the department shall be responsible or liable for any loss, damage or injury arising from the use of or reliance on any information, data or advice (including incomplete, out of date, incorrect, inaccurate or misleading information, data or advice) expressed or implied in, or coming from, this publication or incorporated into it by reference, by any person whosoever.

Further details of geoscience products are available from:

Information Centre
Department of Mines, Industry Regulation and Safety
100 Plain Street
EAST PERTH WA 6004
Telephone: +61 8 9222 3459 | Email: publications@dmirs.wa.gov.au
www.dmirs.wa.gov.au/GSWApublications